Adsorption of aqueous Cd(II) over a Fe_3O_4/plant polyphenol magnetic material

Xiaoxue Jiang, Yuan Zhao, Xiaoyu Wang, Lijun Liu, Yuanyuan Wang, Wenwen Zhang, Liyang Jiao and Wenyan Liang

ABSTRACT

A magnetic plant polyphenol (PP)-coated Fe_3O_4 material (Fe_3O_4/PP) was synthesized and removed Cd(II) from aqueous solution. The structure, morphology, magnetic properties, and thermal stability of the magnetic composite were studied by field emission scanning electron microscopy (FE-SEM), vibrating sample magnetometry (VSM), thermogravimetric analysis (TGA), Fourier transform infrared spectroscopy (FT-IR), X-ray photoelectron spectroscopy (XPS), and zeta-potential measurements. The effect of different parameters (e.g. pH, initial metal ion concentration, contact time, adsorbent dosage, agitation speed, and coexisting ions) on the adsorption process was studied. The adsorption fitted well to the Langmuir isotherm and the adsorption capacity of Cd(II) reached maximum at 0.951 mg/g. The adsorption equilibrium was reached in 2 h and the adsorption kinetic was fitted better to the pseudo-second order equation. The adsorption capacity increased with the pH in the 3.0–8.0 range. Unlike NO_3^- and SO_4^{2-}, common coexisting cations such as Na^+, K^+, Mg^{2+}, and Cl^- negatively affected Cd(II) adsorption. Thermodynamic parameters such as free energy (ΔG), enthalpy (ΔH), and entropy (ΔS) showed that the adsorption process was spontaneous and endothermic. As revealed by FT-IR and XPS, PP and Cd(II) interacted mainly via generation of CdO, CdO_2, or $Cd(OH)_2$ species after Cd(II) adsorption. This study successfully changes the way that PP is used in the removal of Cd(II) and indicates an effective desorption and regeneration performance.

Key words | adsorption, Cd(II), Fe_3O_4, magnetic material, plant polyphenol

Xiaoxue Jiang
Yuan Zhao
Xiaoyu Wang
Lijun Liu
Yuanyuan Wang
Wenwen Zhang
Liyang Jiao
Wenyan Liang (corresponding author)
Beijing Key Lab for Source Control Technology of Water Pollution, College of Environmental Science and Engineering,
Beijing Forestry University,
No. 35 Tsinghua East Road Haidian District, Beijing 100083,
China
E-mail: *lwy@bjfu.edu.cn*

INTRODUCTION

Heavy metals have attracted great attention as they represent threats to public health and aquatic ecological systems (Singh *et al.* 2014). Cadmium is normally found in wastewater derived from industrial activities such as electroplating, solders, batteries, television sets, ceramics, photography, insecticides, electronics, metal-finishing, and metallurgy (Gautam *et al.* 2015). The harmful effects of exposure to certain concentrations of Cd(II) include acute and chronic disorders of the kidney and liver as well as the nervous and cardiovascular systems (Zeng *et al.* 2015). The world-shaking 'itai-itai' disease in Japan was caused by Cd ingestion resulting in multiple fractures due to osteomalacia (Gautam *et al.* 2014). Thus, Cd is considered a very toxic heavy metal.

In order to effectively remove Cd(II), a variety of methods such as chemical precipitation, ion exchange, flotation, reverse osmosis, and electrochemical treatment have been proposed (Shah *et al.* 2016). One of the most promising and frequently used techniques, the adsorption method, has received attention because of its high efficiency, economy, and effectiveness (Machida *et al.* 2012), and common adsorbents include activated carbons (Demiral & Güngör 2016), clays (Roque-Ruiz *et al.* 2016), and polymeric materials (Silva & Pissetti 2014).

doi: 10.2166/aqua.2018.051

Plant polyphenols (PP), or tannin, are inexpensive and ubiquitous natural polymers derived from vegetal secondary metabolites of higher plants (Morisada *et al.* 2011). PP can be found in almost every part of higher plants (e.g. bark, wood, leaves, fruit, and roots) (Wang *et al.* 2013). As a natural material, PP is produced in large quantities. PP has been manufactured as an important commercial material, with a large number of applications (e.g. tanning agents, adhesives, cosmetics, pharmaceuticals, and food) (Ping *et al.* 2011; Wang *et al.* 2013).

PP is usually classified into two groups, namely hydrolysable and condensed (also named non-hydrolysable) tannin (Morisada *et al.* 2011). Because of the presence of multiple adjacent phenolic hydroxyls in the molecular structure, PP exhibits a specific affinity towards numerous metal ions such as Cu(II), Pb(II), and Cr(VI) (Xu *et al.* 2017). Therefore, PP can remove metal ions and become an effective alternative adsorbent. However, the common condensed type of tannin, such as *Larix gmelinii*, bayberry, black wattle and persimmon tannin, is water soluble, which makes it difficult to separate from solution after interacting with metal ions (Huang *et al.* 2009; Xie *et al.* 2016; Xu *et al.* 2017). In order to remove aqueous heavy metals, PP requires immobilization or insolubilization processes before being used. PP can be prepared in the form of gels, resins, and immobilized on other matrices (Bacelo *et al.* 2016). Polyphenol–SiO_2 hybrid biosorbent, bayberry tannin-immobilized collagen fiber, persimmon waste gel, and modified quebracho tannin resin, which are all rich in phenolic hydroxyls, can be used to remove Hg(II), Pb(II), and Cr(VI) (Huang *et al.* 2009; Yurtsever & Sengil 2009; Inoue *et al.* 2010; Copello *et al.* 2013). Metal adsorption on PP normally involves physicochemical interactions (e.g. electrostatic force, ion exchange, metal-ion chelation, or complexation) between the adsorbate and the adsorbent (Dodson *et al.* 2015). However, separation of PP adsorbents (gel, resin, or immobilized on matrices) often needs filtration or centrifugation, which may result in adsorbent losses and secondary pollution.

Magnetic adsorbents such as iron oxide materials show excellent properties and have received considerable interest because of their easy separation and regeneration (Chang *et al.* 2016). Magnetite (Fe_3O_4) is a ferromagnetic compound with superior magnetic properties compared with other metallic compounds. With the aim of providing magnetic adsorbents with high adsorption capacity and specific metal complexation characteristics, a number of surface modification techniques have been developed via coating with different surface stabilizers. In this sense, a good number of materials including MnO_2, SiO_2, bentonite, and polymers have been reported to be suitable for modifying the surface of Fe_3O_4. In particular, natural polymers (e.g. chitosan, starch and its derivatives), which have received significant attention, have unique physicochemical characteristics, low cost, natural abundance, and multiple reactive groups in the molecule (Crini 2005).

In this study, a magnetic Fe_3O_4 material coated with PP (Fe_3O_4/PP) was synthesized to overcome the difficulty in separating immobilized PP adsorbents and removed aqueous Cd(II). The combination of PP with magnetic Fe_3O_4 could induce effective functional groups and obtain rapid separation of the adsorbent from wastewater. The surface structure, morphology, and magnetic properties of Fe_3O_4/PP were analyzed using field emission scanning electron microscopy (FE-SEM), and vibrating sample magnetometry (VSM). The thermal stability was determined by thermogravimetric analysis (TGA). The effect of some factors, such as pH, contact time, initial metal ion concentration, adsorbent dosage, agitating speed, and coexisting ions, on the adsorption process was studied. The relevant mechanisms governing the adsorption of Cd(II) on Fe_3O_4/PP were investigated by kinetics (i.e. pseudo first-order and pseudo second-order), adsorption isotherm modelling (i.e. Langmuir and Freundlich), and thermodynamics analyses based on the experimental data. In particular, the surface properties of the Fe_3O_4/PP–Cd(II) composite formed after Cd(II) adsorption were analyzed by Fourier transform infrared spectroscopy (FT-IR) and X-ray photoelectron spectroscopy (XPS).

MATERIALS AND METHODS

Materials

Raw PP powder (extracted from the bark of *Larix gmelinii*) was purchased from the Inner Mongolia Forestry Industrial Co., Ltd (Yakeshi, China). The naked Fe_3O_4 powder, produced from a natural magnetite ore, was obtained from Baotou Bally Ken Industrial Technology Co., Ltd (Baotou,

China). Analytical-grade cadmium nitrate [$Cd(NO_3)_2{\cdot}4H_2O$] was obtained from the Institute of Jinke Fine Chemicals (Tianjin, China). Other chemical reagents used herein were of analytical grade and used without further purification.

Preparation of Fe_3O_4/PP composite

The PP powder was first purified following the method according to Wang *et al.* (2013). Briefly, 20 g of PP were dissolved in 300 mL of distilled water. The resulting PP solution was centrifuged, extracted, purified, and condensed via rotary evaporation. A purified PP powder was obtained by freeze-drying the above concentrated solution. After purification, the PP content increased from 34.9 to 44.2%. The naked Fe_3O_4 was washed with distilled water three times and subsequently dried at room temperature. The purified PP was dissolved in distilled water and the final concentration was 12.5 g/L. The Fe_3O_4/PP composite was synthesized by mixing 1.0 g of Fe_3O_4 particles with 40 mL of the PP solution for 2 h at room temperature. Using an external magnet, the Fe_3O_4/PP particles were separated from the solution and washed twice with 10 mL distilled water. The Fe_3O_4/PP composite was freeze-dried and stored at 4 °C.

Preparation of the Cd solution

The concentration of Cd(II) stock solution was 200 mg/L and dissolved [$Cd(NO_3)_2{\cdot}4H_2O$] in ultrapure water (18 MΩ/cm) containing 0.03 mol/L of HNO_3. The Cd(II) concentrations needed in each adsorption experiment were achieved by diluting the above stock solution.

Characterization of the materials

The mixture of PP and KBr at 1:100 (m:m) was pressed using a tableting machine for 15 s, and then was recorded on a Fourier transform infrared spectrometer (VERTEX 70, Bruker, Germany) from 400 to 4,000 cm^{-1} with a resolution of 4 cm^{-1}. The morphology of the Fe_3O_4/PP composite, which was directly adhered to the sample stage with a conductive paste, was examined on a field emission scanning electron microscope (QUANTA 200 F, FEI Technologies, USA). The magnetic properties were determined with a vibrating sample magnetometer (LakeShore 7410, Lake Shore Cryotronics, USA) at room temperature under a magnetic field of ±2.0 T. The thermal stability of Fe_3O_4/PP was evaluated on a thermogravimetric analyzer (TGA Q50, TA Instruments-Waters LLC, USA) up to 800 °C and heating rate set to 10 °C/min. The X-ray diffraction (XRD) patterns were recorded on a Rigaku Dmax/2400 X-ray diffractometer (RINT 2000, Rigaku, Japan) equipped with a graphite monochromatized Cu Kα ($\lambda = 0.1542$ nm) source operating at 40 kV and 80 mA and with a scanning rate of 0.02°/min (2θ: 10–80°). The solid sample of XRD was added to an agate mortar and then placed in a sample stage for measurement after being uniformly ground. XPS analysis was carried out on an X-ray photoelectron spectroscope (PHI Quantera SXM, ULVAC-PHI, Japan) equipped with a monochromated X-ray source (Al-Kα, 1,486.6 eV photon energy) as the excitation source. The sample of XPS was spread on an aluminum foil with tape and covered with another piece of aluminum foil, and then pressed using a tableting machine for 10 s.

Adsorption kinetics and isotherms

The adsorption kinetics were investigated in 500 mL conical flasks with 300 mL of Cd(II) solution at varying concentrations (5, 20, and 40 mg/L). After adjusting the pH to 7.0 by adding 0.1 M HNO_3 and NaOH, 3.0 g Fe_3O_4/PP were added to the Cd(II) solution. After a magnet was put at the bottom of the flasks, the aliquots were taken at determined time intervals (from 10 min to 1 h) and then filtered using a 0.45 μm water membrane. Finally, the filtrate concentration of Cd(II) was measured on an AA-6300 atomic absorption spectrophotometer (AAS, Shimadzu, Japan) provided with an air-acetylene burner.

The adsorption isotherm experiments set a series of different initial Cd concentrations and were carried out at 298 K. The dosage of Fe_3O_4/PP for varying concentrations of Cd(II) solution (50 mL, 2–40 mg/L) was fixed (0.5 g) and the pH value was adjusted to 7.0. The rotary shaker speed was fixed to 160 rpm and the adsorption system approached equilibrium after shaking for 2 h. All samples were filtered with a 0.45 μm water membrane and the Cd (II) concentration of the filtrates was analyzed by AAS. The adsorption thermodynamics study was conducted at three different temperatures (288, 298, and 308 K).

After measuring the Cd(II) concentration by AAS, the removal efficiency and the adsorption capacity were calculated using Equations (1) and (2), respectively:

$$\text{Removal efficiency } (\%) = \frac{C_0 - C_t}{C_0} \times 100\% \quad (1)$$

$$q_t = \frac{(C_0 - C_t) \times V}{m} \quad (2)$$

where C_0 (mg/L) and C_t (mg/L) are the initial concentration of Cd(II) and the concentration of Cd(II) at different time intervals, respectively; V (L) is the volume of the solution; m (g) is the mass of the adsorbent; and q_t (mg/g) is the Cd(II) adsorption capacity of the adsorbent at different time intervals.

Adsorption experiments

To investigate the influence of different parameters on the adsorption process, the effect of some operating parameters (e.g., pH, adsorbent dose, agitation speed, and common coexisting ions) was studied. The pH of the solution ranged from 3.0 to 8.0 by adding 0.1 M HNO_3 or NaOH aqueous solutions; 0.5 g of Fe_3O_4/PP were added to 50 mL Cd(II) solution and the concentration was 20 mg/L. The mixture was agitated at 298 K by a rotary shaker at 160 rpm for 8 h. The effect of adsorbent dosage was performed by using 50 mL of a 20 mg/L Cd(II) solution at pH 7.0. The adsorbent dosage varied from 0.5 to 3.0 g, while the agitation speed was maintained at 160 rpm for 8 h and a temperature of 298 K. To determine the effect of the agitation speed, 0.5 g of Fe_3O_4/PP were added to Cd(II) solution (50 mL, 20 mg/L) at pH = 7.0, and the agitation speed ranged from 50 to 250 rpm for 8 h at 298 K. Common coexisting ions were added at three concentration levels (5, 20, and 40 mg/L) by using Na^+, K^+, Mg^{2+}, Cl^-, NO_3^-, and SO_4^{2-} ion solution. For these experiments with concentration levels, 50 mL of a 20 mg/L Cd(II) solution was used at constant Fe_3O_4/PP dosage (0.5 g), pH (7.0), agitation speed (160 rpm), and temperature (298 K) for 8 h. At each equilibrium time, Fe_3O_4/PP was separated from the upper solution with a magnet. The obtained sample solutions were filtered with a syringe filter containing a 0.45-μm water membrane. The Cd(II) concentration of the supernatant was measured by AAS. The Fe_3O_4/PP–Cd(II) complexes obtained after Cd(II) adsorption were analyzed by FT-IR and XPS spectra.

Statistical analysis

Analysis of variance (ANOVA) and least significant differences (LSD) were performed for statistical analysis using software SPSS 18.0 (SPSS Inc., Chicago, USA). The results were considered significant at a significance value (p-value) <0.05.

RESULTS AND DISCUSSION

Characterization

The surface morphology of the naked Fe_3O_4 and Fe_3O_4/PP was characterized by FE-SEM. As shown in Figure 1, both the naked Fe_3O_4 and Fe_3O_4/PP materials showed a very rough morphology. Fe_3O_4 did not show significant morphology and structural changes after PP coating. Large domains formed by blocky-shaped particles were observed, and this may result from the uneven particle size of natural magnetite. Overall, PP was bonded to the surface of Fe_3O_4 without changing the morphology and structure of Fe_3O_4.

Figure 2 shows a typical S-type magnetic hysteresis of the naked Fe_3O_4 and Fe_3O_4/PP materials. The corresponding magnetization saturation (Ms) values of the naked Fe_3O_4 and Fe_3O_4/PP were 61.3 and 59.1 emu/g, respectively. PP, being a polymer, was diamagnetic and this explained the slightly lower saturation magnetization of the coated material. The remanent magnetization (Mr) and coercivity (Hc) of the naked Fe_3O_4 and Fe_3O_4/PP (right inset, Figure 2) were $Mr = 6.22$ and 5.09 emu/g and $Hc =$ 67.22 and 70.21 Oe, respectively. Mr and Hc were nonzero values, revealing ferromagnetic properties for both Fe_3O_4 and Fe_3O_4/PP. The high magnetism showed by Fe_3O_4/PP after the coating process allowed quick separation from the liquid phase with an external magnet.

The TGA profiles of the naked Fe_3O_4 and Fe_3O_4/PP materials were obtained to investigate their thermal properties. The percentage of weight loss of different materials

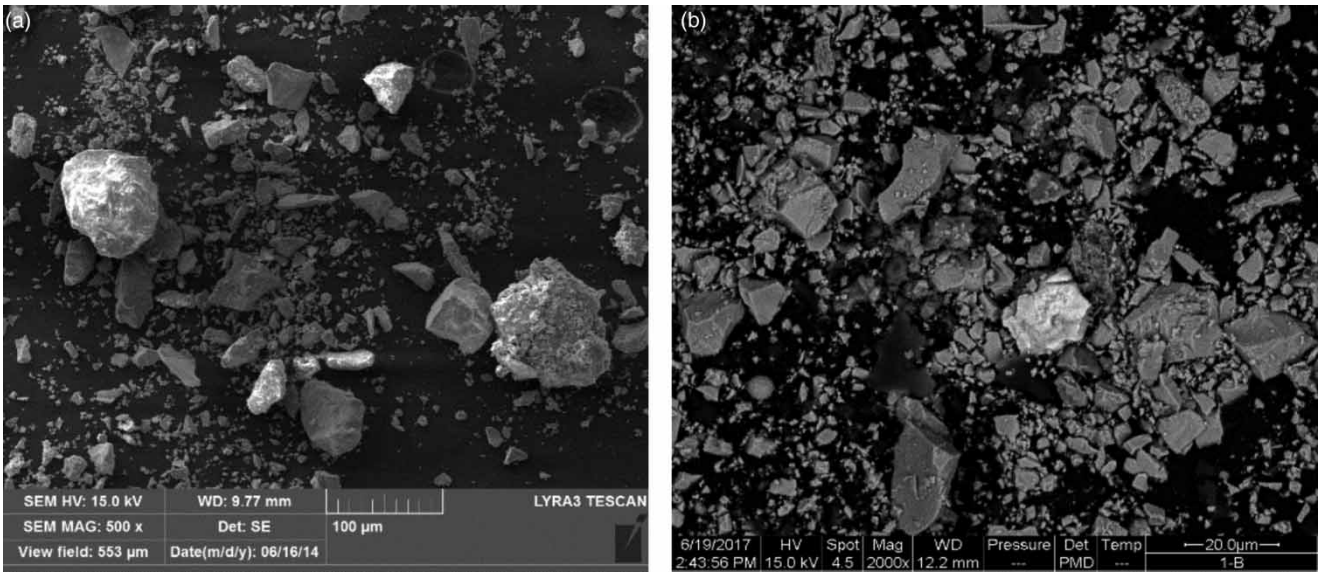

Figure 1 | FE-SEM images of the naked (a) Fe_3O_4 and (b) Fe_3O_4/PP materials.

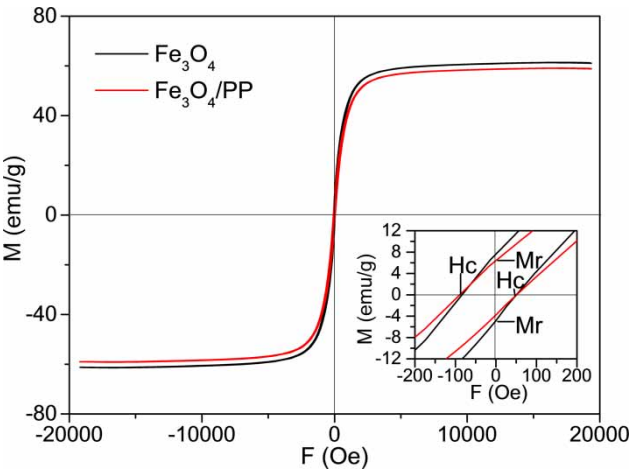

Figure 2 | Magnetization curves of the naked Fe_3O_4 and Fe_3O_4/PP materials.

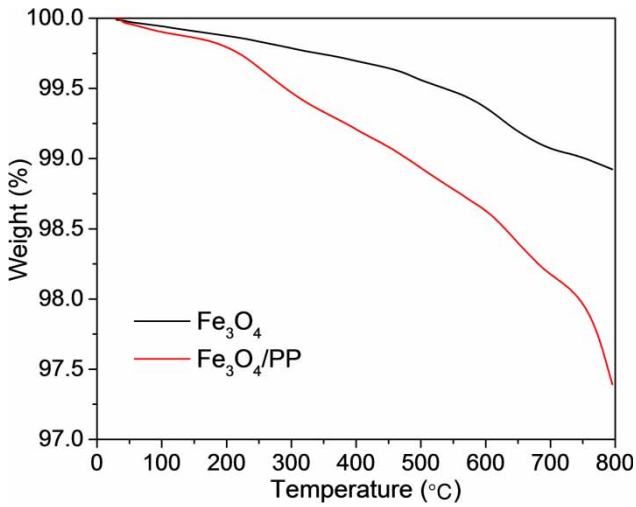

Figure 3 | TGA curves of the naked Fe_3O_4 and Fe_3O_4/PP materials.

increases with increasing temperature. Therefore, the TGA curve can express the thermal stability of the sample and the coating amount of the material. As depicted in Figure 3, Fe_3O_4 showed a weight loss of only 0.13% from 28 to 200 °C due to release of physically adsorbed water, while the weight loss from 200 to 600 °C may result from the decomposition of the crystalline structure. A weight loss of 0.44% was obtained in the 600–800 °C range, and this weight loss was related to the decomposition of the magnetite residue and the thermal decomposition of the crystal. This slight mass loss was indicative of the good thermal stability of Fe_3O_4. With regard to Fe_3O_4/PP, the initial weight loss (0.21%) in the 28–200 °C range was produced by the release of water. An increase in temperature to 300 °C resulted in weight loss produced by the decomposition of organic compounds of the PP coating. The mass loss linearly decreased with temperature up to 800 °C, indicating that the PP was firmly anchored onto the Fe_3O_4 surface. As revealed by the weight of the material at 800 °C, PP was decomposed and carbonized at this temperature. The PP on the surface of the Fe_3O_4 also began to decompose when the

temperature exceeded 120 °C (Wang *et al.* 2018). This indicated that the activity of the prepared Fe_3O_4/PP particles was not affected unless at high temperature. A comparison of the TGA curves of Fe_3O_4 and Fe_3O_4/PP revealed a PP coating loading of approximately 1.53%.

XRD was used to determine the crystalline structure and provided physical-chemical information on the PP coated on the magnetic material. Figure 4 shows that PP generated a broad peak at 21°, indicating its amorphous nature (He *et al.* 2012). For Fe_3O_4, the characteristic peaks agreed well with the standard XRD pattern of the JCPDS (No.74-0748) card. The XRD pattern of Fe_3O_4 showed seven peaks at 18.29, 30.08, 35.44, 43.06, 53.43, 56.96, and 62.54°, corresponding to Miller indices of (111), (220), (311), (400), (422), (333), and (440), respectively, typical of a cubic inverse spinel structure (Venkateswarlu & Yoon 2015). Similar peaks were observed for the Fe_3O_4/PP, suggesting that the coating of PP did not result in any phase change of Fe_3O_4.

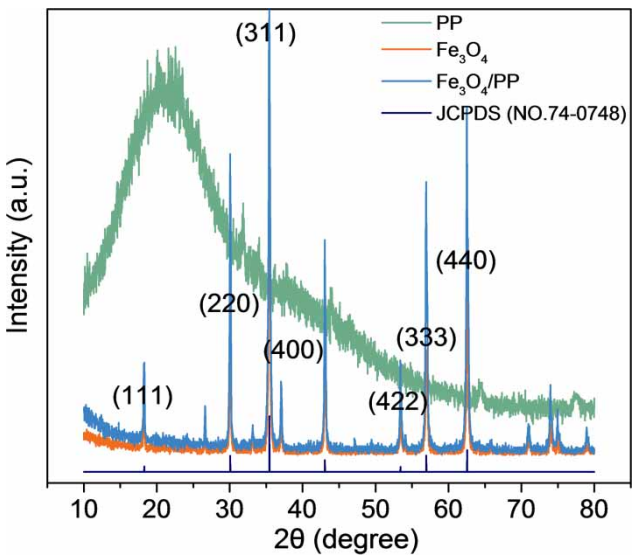

Figure 4 | XRD patterns of PP, the naked Fe_3O_4 and Fe_3O_4/PP materials.

Adsorption kinetics and isotherms

With the aim of obtaining the equilibrium time for the maximum adsorption capacity, Figure 5(a) shows the effect of the contact time on the adsorption of Cd(II). Adsorption was fast from 10 to 60 min and gradually slowed down. The adsorption equilibrium was reached within 2 h. Obviously, the adsorption of Cd(II) had significant influence on contact time ($p < 0.05$). The amounts of Cd(II) adsorbed on Fe_3O_4/PP at equilibrium ($q_{e,exp}$) were 0.419, 0.749, and 0.921 mg/g when Cd(II) concentration was 5, 20, and 40 mg/L, respectively. The rapid adsorption rate can be ascribed to the strong chelating interaction between the surface functional groups of PP and Cd(II). To ensure that equilibrium was completely reached, the subsequent experiments were carried out for a longer time (8 h).

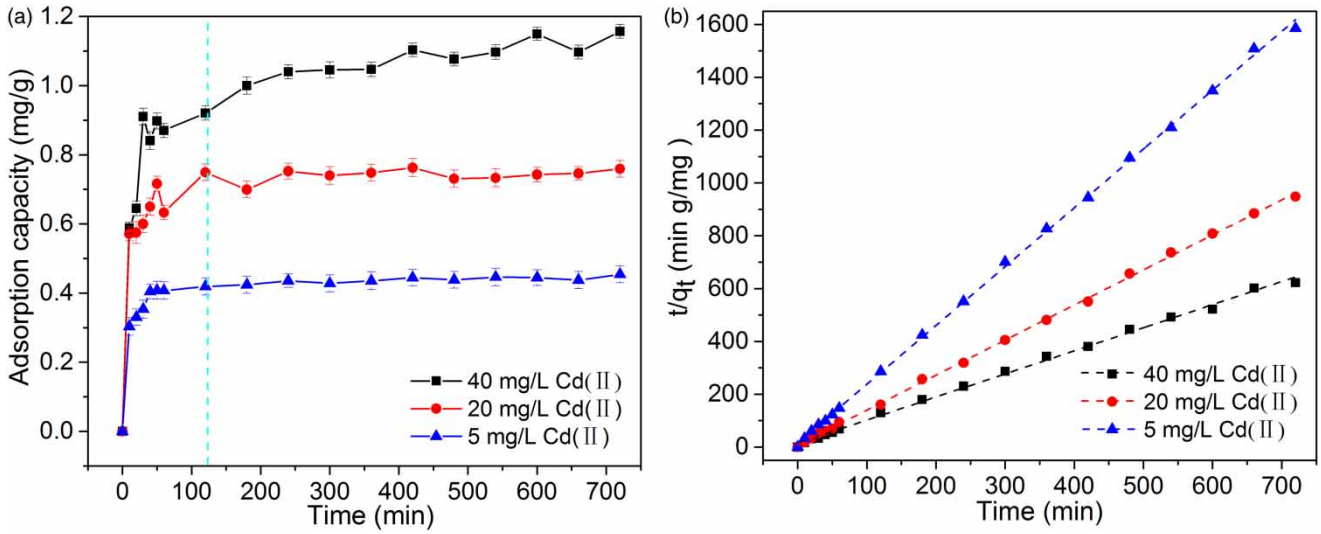

Figure 5 | (a) Effect of the contact time on the adsorption of Cd(II) and (b) the pseudo second-order plots (initial pH = 7.0, adsorbent dose = 3.0 g, contact time = 12 h, temp. = 298 K).

Table 1 | Kinetic parameters for the adsorption of Cd(II) on Fe_3O_4/PP (pH 7.0, Cd(II) = 20 mg/L, adsorbent dose = 3.0 g, contact time = 12 h, temp. = 298 K)

	Pseudo first-order model			Pseudo second-order model			
Initial concentration of Cd(II) (mg/L)	k_1 (min^{-1})	$q_{e,cal}$ (mg/g)	R^2	k_2 (g/mg/min)	$q_{e,cal}$ (mg/g)	h (mg/g/min)	R^2
5	0.0024	0.743	0.708	0.0132	0.449	0.0027	0.999
20	0.0022	0.523	0.589	0.0778	0.754	0.0442	0.999
40	0.0036	0.369	0.778	0.0878	1.144	0.1150	0.997

Note: $q_{e,cal}$ is the equilibrium adsorption capacity calculated by the kinetic models.

The kinetic study can predict the adsorption mechanism, which is important for adsorption of Cd(II). Therefore, two common kinetic models, namely the pseudo first-order model and pseudo second-order model, were used to fit the experimental data, and the linear equations of the two models are expressed in Equations (3) and (4), respectively:

$$\log(q_e - q_t) = \log q_e - \left(\frac{k_1}{2.303}\right)t \tag{3}$$

$$\frac{t}{q_t} = \frac{1}{k_2 q_e^2} + \left(\frac{1}{q_e}\right)t \tag{4}$$

where q_e and q_t are the amounts of adsorbed Cd(II) (mg/g) at equilibrium and at time t (min), respectively; k_1 (1/min) and k_2 (g/mg/min) are the rate constants of the pseudo first-order model and pseudo second-order model, respectively; and $h = k_2 q_e^2$ is the initial adsorption rate. Figure 5(b) shows the linear pseudo second-order plot, while Table 1 summarizes the kinetic parameters. The values of k_2 and $q_{e,cal}$ can be calculated from the t/q_t versus t plot. Comparing the R^2 values, the adsorption kinetic of Cd(II) was more in line with a pseudo second-order kinetic model. This result suggested that the adsorption process was controlled by the chemical adsorption, involving valence forces upon sharing or exchange of electrons (Xu *et al.* 2012). In addition, the $q_{e,exp}$ values were more comparable to the values calculated by the pseudo second-order kinetics; ($q_{e,cal}$). h increased with Cd(II) from 5 to 40 mg/L, indicating that the adsorption rate increased with this parameter. Mimosa tannin immobilized on collagen or PP immobilized within a SiO_2 matrix required 24 h or longer to reach heavy metal adsorption equilibrium (Kim *et al.* 2012; Copello *et al.* 2013). Compared with these adsorbents, Fe_3O_4/PP showed a faster adsorption rate and equilibrium was reached in only 2 h.

The adsorption isotherms reflect the affinity between an adsorbent and an adsorbate at a particular temperature. Thus, it is necessary to study the adsorption at equilibrium via the isotherm equation. As shown in Figure 6(a), the removal capacity increased with the initial Cd(II) concentration (2–20 mg/L) and levelled off thereafter (above 25 mg/L), gradually reaching the saturation capacity of Fe_3O_4/PP. From statistical analysis, there was a significant difference when the concentration was less than 20 mg/L ($p < 0.05$). When the initial Cd(II) concentration was 20 mg/L, the saturated adsorption capacity of Fe_3O_4/PP was 0.722, 0.797, and 1.068 mg/g at 288, 298, and 308 K, respectively. Moreover, the three temperatures all had significant differences for the adsorption of Cd(II) ($p < 0.05$).

In order to understand the distribution of Cd(II) between the liquid–solid phases, it is necessary to study the adsorption isotherms by using the Langmuir and Freundlich isotherm models. The assumption of the Langmuir isotherm is based on monolayer adsorption of ions on homogeneous surface sites, whereas the assumption of the Freundlich isotherm is based on multilayer adsorption on heterogeneous surface sites. The linear equations of the Langmuir and Freundlich isotherm models are expressed in Equations (5) and (6), respectively.

$$\frac{C_e}{q_e} = \frac{1}{K_L q_m} + \frac{C_e}{q_m} \tag{5}$$

$$\log q_e = \frac{1}{n}\log C_e + \log K_F \tag{6}$$

where C_e (mg/L) is the equilibrium concentration; q_e (mg/g) is the amount of Cd(II) adsorbed at equilibrium;

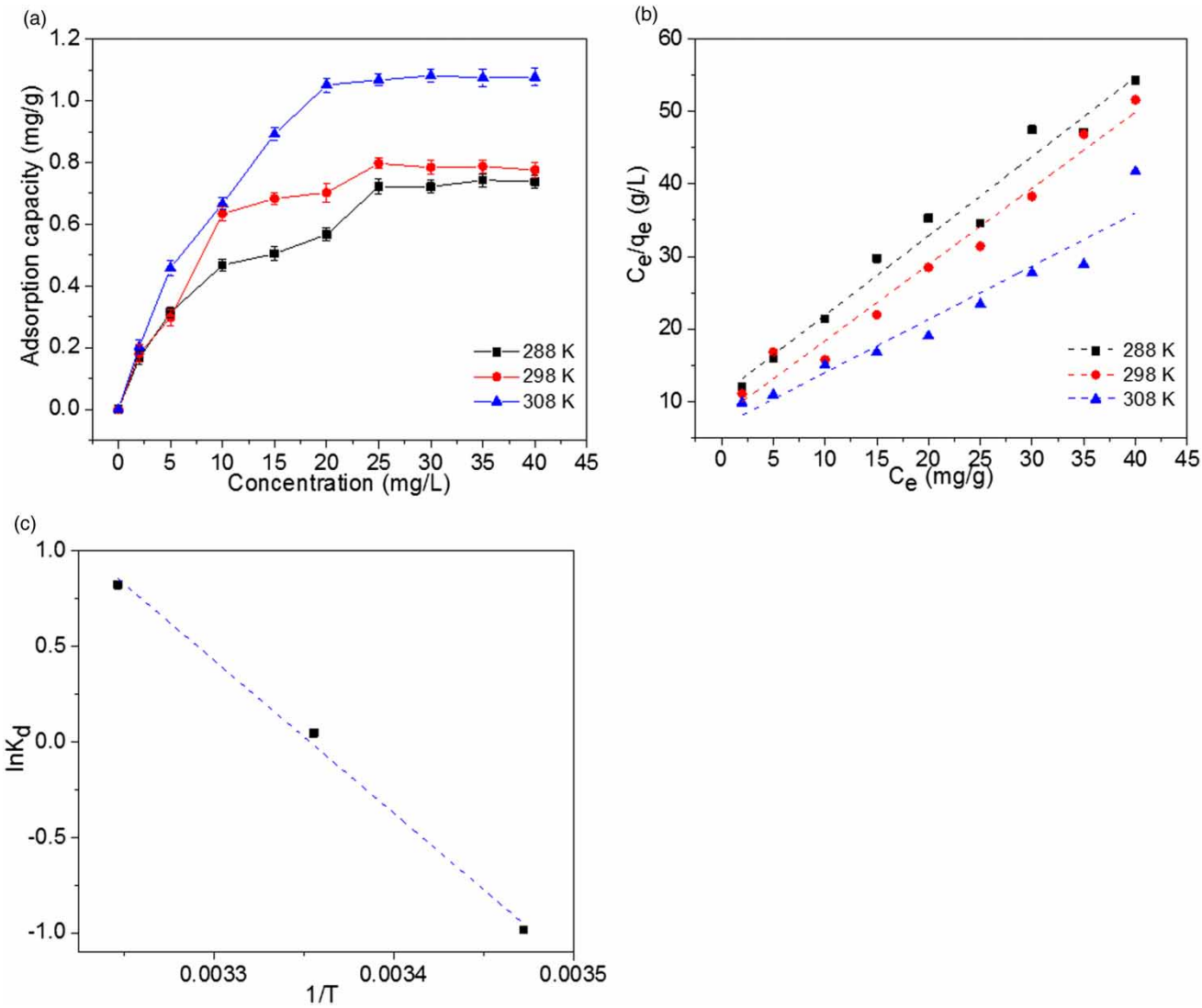

Figure 6 | (a) Effect of the initial concentration of Cd(II) on the adsorption of Cd(II), (b) Langmuir isotherm linear plots, and (c) thermodynamic linear plot lnK_d vs 1/T (initial pH = 7.0, Cd(II) concentration = 2–40 mg/L, adsorbent dose = 0.5 g, contact time = 8 h, temp. = 298 K).

q_m (mg/g) is the maximum adsorption capacity of the monolayer; K_L (L/mg) is the Langmuir constant (related to the affinity and the adsorption energy); K_F and n represent Freundlich constants and intensity factors (associated with adsorption intensity), respectively. The parameters and fitting plots are shown in Table 2 and Figure 6(b), respectively. The R^2 values of the Langmuir and Freundlich models were 0.971 and 0.805 at 298 K, revealing a better fit to the Langmuir equation. From the slope and intercept of the linear C_e/q_e against C_e plot q_m and K_L are obtained, respectively. According to the Langmuir model, the maximum adsorption amount calculated was 0.951 mg/g at 298 K, which was close to the experimental value. Moreover, K_L increased with temperature, indicating that a higher temperature was more favorable for Cd(II) adsorption. The adsorption system followed the Langmuir isotherm model, indicating that the adsorption was a monolayer coverage and the adsorption sites were equal and homogeneous.

To further confirm the affinity between the adsorbate and the adsorbent, a dimensionless constant separation

Table 2 | Adsorption parameters for the Langmuir and Freundlich isotherm models and the thermodynamics parameters for the adsorption of Cd(II) on Fe_3O_4/PP at different temperatures (pH 7.0, Cd(II) = 2–40 mg/L, adsorbent dose = 0.5 g, contact time = 8 h, temp. = 298 K)

	Langmuir				Freundlich					
Temp. (K)	K_L (L/mg)	q_m (mg/g)	R_L	R^2	K_F	1/n	R^2	ΔG (KJ/mol)	ΔH (KJ/mol)	ΔS (J/(mol·K))
288	0.083	0.914	0.375	0.970	0.134	0.486	0.959	2.35	66.59	223.29
298	0.121	0.951	0.255	0.971	0.156	0.469	0.805	−0.11		
308	0.205	1.364	0.196	0.919	0.170	0.555	0.908	−2.10		

factor (R_L) can be defined as:

$$R_L = \frac{1}{1 + K_L C_0} \tag{7}$$

where C_0 is the concentration of Cd(II) (mg/L). The nature of the adsorption process was provided by R_L: irreversible ($R_L = 0$), favorable ($0 < R_L < 1$), linear ($R_L = 1$), and unfavorable ($R_L > 1$). Since R_L lay between 0 and 1 for the three different temperatures, the adsorption of Cd(II) on Fe_3O_4/PP was considered to be favorable and the adsorption equilibrium of Cd(II) on Fe_3O_4/PP was appropriate by the Langmuir model.

Adsorption thermodynamics

The Cd(II) adsorption thermodynamic process was performed at temperatures of 288, 298, and 308 K. Thermodynamics parameters such as the Gibb's free energy (ΔG), the enthalpy change (ΔH), and the entropy change (ΔS) were calculated by the Van't Hoff equation.

$$K_d = \frac{q_e}{C_e} \tag{8}$$

$$\Delta G = -\mathrm{RT} \ln K_d \tag{9}$$

$$\Delta G = \Delta H - T\Delta S \tag{10}$$

where R is the universal gas constant (8.314 J/mol/K); T is the absolute temperature (K); and K_d is the distribution coefficient. The slope and intercept of the lnK_d vs 1/T plot (Figure 6(c)) could calculate ΔH and ΔS, respectively. The relevant parameters at the three temperatures are listed in Table 2. The values of ΔG were negative obtained at 298 and 308 K, indicating that the adsorption of Cd(II) on Fe_3O_4/PP was thermodynamically feasible and spontaneous. It was also shown that the adsorption was not spontaneous at lower temperature (288 K). With increasing temperature from 288 to 308 K, the decrease in ΔG indicated that high temperature was beneficial for the adsorption of Cd(II) (Homayoon *et al.* 2017). The positive ΔH value indicated that the adsorption reaction of Cd(II) was endothermic (i.e., the reaction consumed energy). In addition, as shown in Figure 6(a), with the increase of temperature from 288 to 308 K, the adsorption capacity increased with temperature, in line with the positive ΔH value. The positive value obtained for ΔS demonstrated that the solid–liquid interface randomness increased during Cd(II) adsorption. The positive ΔS value indicated the irreversibility and stability of the Cd(II) adsorption process (Chand *et al.* 2014). In summary, adsorption of Cd(II) on Fe_3O_4/PP was achieved at room temperature and the interaction between Cd(II) and Fe_3O_4/PP was spontaneous.

Effect of pH

Studying the pH value of the metal solution was important and it had an obvious effect on the surface charge and ionic state of the adsorbent (Xu *et al.* 2016). Thus, the pH was investigated in the 3.0–8.0 range. As shown in Figure 7, the adsorption of Cd(II) depended highly on the pH, which had a significant effect on the removal of Cd(II) ($p < 0.05$). Thus, the amount of Cd(II) adsorbed increased sharply from 0.0584 to 0.529 mg/g upon increasing the pH from 3.0 to 5.0 and increased slowly thereafter (pH = 5.0–7.0). The maximum adsorption was obtained at pH = 7.0 and decreased thereafter with pH increasing to 8.0. The K_{sp} of Cd(II) (4.47×10^{-15} at 25 °C) indicates that Cd(II) can

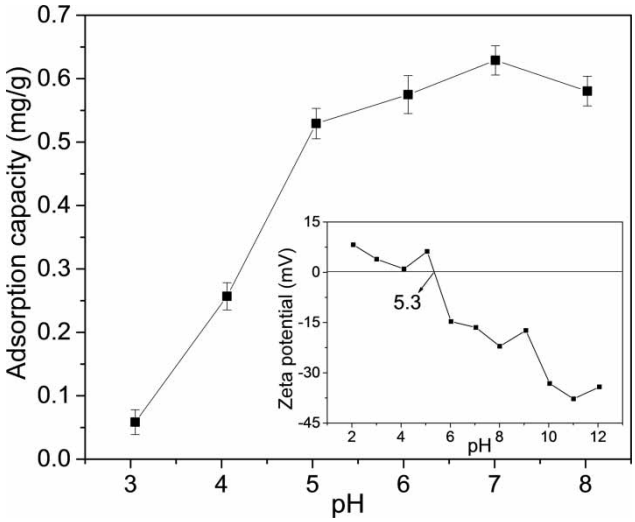

Figure 7 | Effect of the pH on the adsorption of Cd(II) (initial pH = 3.0–8.0, Cd(II) concentration = 20 mg/L, adsorbent dose = 0.5 g, contact time = 8 h, temp. = 298 K).

form solid metal hydroxide precipitates at pH higher than 8.0. Thus, the experiments carried out herein were limited to the 3.0–8.0 range of pH.

Since Cd^{2+} is the predominant species in the 3.0–8.0 pH range, the distribution of Cd(II) species at different pH values had a negligible effect on the adsorption capacity (i.e. the surface charge of Fe_3O_4/PP controlled the effect of the pH). In addition, the pH observably determined the degree of deprotonation of the phenolic hydroxyls of PP. These groups can chelate with metal ions to form five-member chelating ring species (Kim *et al.* 2012). The degree of deprotonation of the adsorbent can be further explained by the surface charge of Fe_3O_4/PP and the point of zero charge (pzc). From the inset of Figure 7, Fe_3O_4/PP showed a pH_{pzc} of 5.3. When $pH < pH_{pzc}$, Fe_3O_4/PP was positively charged such that cationic Cd(II) species were electrostatically repelled. At lower pH values, H^+ was in higher concentration and Cd(II) ions and H^+ competed for the available adsorption sites, thereby additionally hindering Cd(II) adsorption. When $pH > 5$, the adsorption of Cd(II) was favored because the adsorbent was negatively charged (i.e. a higher number of phenolic hydroxyls on PP were ionized). As a result, the electrostatic attraction between Fe_3O_4/PP and Cd(II) ions increased, resulting in the formation of Cd–ligand magnetic complexes. The adsorption capacity of bayberry or black wattle tannin increased with the pH of the solution (Huang *et al.* 2009; Xu *et al.* 2017). The larch tannin (a condensed tannin) used herein also contains multiple adjacent phenolic hydroxyls, which acted as the main complexing sites for Cd(II).

Effect of the adsorbent dose and the agitating speed

To investigate the effect of the adsorbent dose, the adsorbent dosage varied from 0.5 to 3.0 g. As shown in Figure 8(a), the removal percentage increased gradually with the mass of adsorbent, mainly due to the higher number of active sites that were available for the removal of Cd(II) (El-Hamshary *et al.* 2014). It can be seen that, with the amount of Fe_3O_4/PP increasing from 0.5 to 3.0 g, the removal of Cd(II) significantly increased ($p < 0.05$) from 36.6 to 96.3% and the adsorption capacity significantly decreased ($p < 0.05$) from 0.734 to 0.400 mg/g. At lower adsorbent dosage, the number of active adsorption sites was limited and Cd(II) competed with the functional groups for these sites. When the amount of adsorbent was further increased to 3.0 g, the removal percentage reached a maximum and the number of active adsorption sites nearly reached saturation value. This phenomenon, whereby the removal percentage increases gradually to saturation with the increase of adsorbent dose, has also been observed for other adsorbents (e.g. cashew nut shell resin and hydrous manganese dioxide) (Zhai & Wang 2015; Devi *et al.* 2017).

The effect of the agitation speed was investigated by changing within the 50–250 rpm range. As shown in Figure 8(b), the adsorption capacity increased from 0.267 to 0.665 mg/g upon increasing from 50 to 200 rpm. When setting the agitation speed at 250 rpm, the adsorption capacity decreased to 0.587 mg/g. Overall, there were significant differences ($p < 0.05$) in the range of 50–200 rpm while 250 rpm exhibited no significant difference ($p > 0.05$) compared with other agitation speeds. This result can be explained in two aspects. On the one hand, increasing the agitation speed resulted in higher convective mass transfer of metal ions from the bulk solution. On the other hand, higher agitation speed decreased the boundary layer resistance close to the adsorbent surfaces (Murithi *et al.* 2014). In the case of the study herein, agitation made the contact of the metal ions with the surface of the adsorbent more sufficient, increasing the amount of Cd(II) adsorbed as a result.

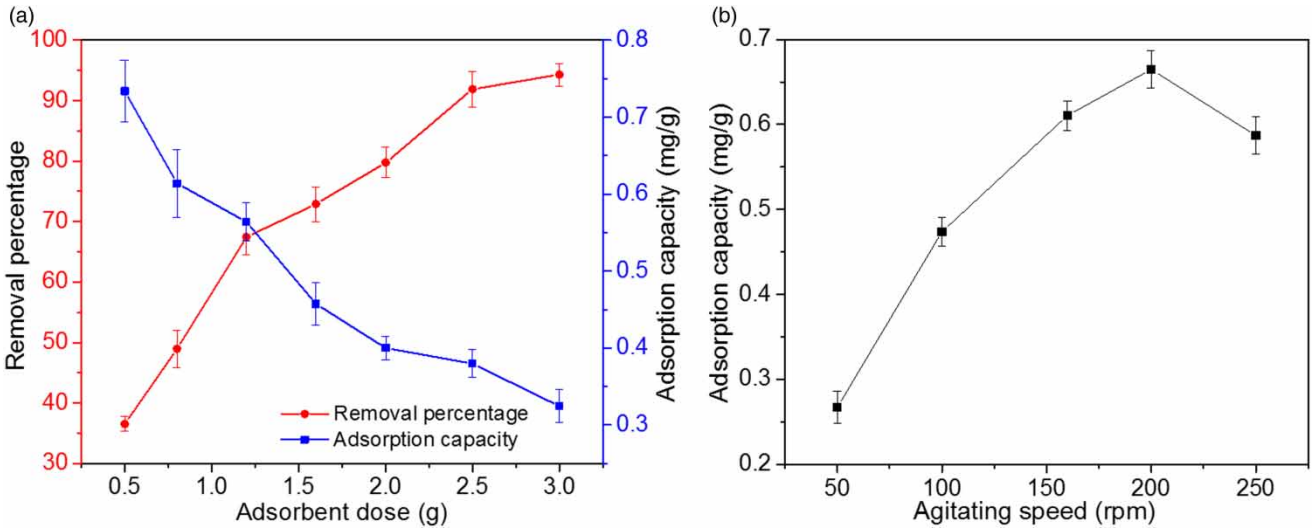

Figure 8 | (a) Effect of the adsorbent dose and (b) the agitating speed on the adsorption of Cd(II) (initial pH = 7.0, Cd(II) concentration = 20 mg/L, adsorbent dose = 0.5 g, contact time = 8 h, temp. = 298 K).

Effect of the coexisting ions

The influence of the presence of coexisting cations (e.g. Na^+, K^+, and Mg^{2+}) on the adsorption process is summarized in Figure 9(a). In summary, the presence of Na^+, K^+, and Mg^{2+} hindered the adsorption of Cd(II) at the three ion concentration levels studied herein, which had a significant influence ($p < 0.05$) on the removal percentage compared with the control, this being particularly true for Mg^{2+}. Na^+ significantly inhibited the adsorption of Cd(II) at low concentration (5 mg/L), whereas K^+ and Mg^{2+} reduced the Cd(II) removal percentage at higher concentration (40 mg/L). The influence of the cations followed the trend $Mg^{2+} > K^+ > Na^+$. The removal efficiency decreased upon increasing the K^+ and Mg^{2+} concentrations, since these metal cations competed for the active sites of the adsorbent with Cd^{2+} (Chen

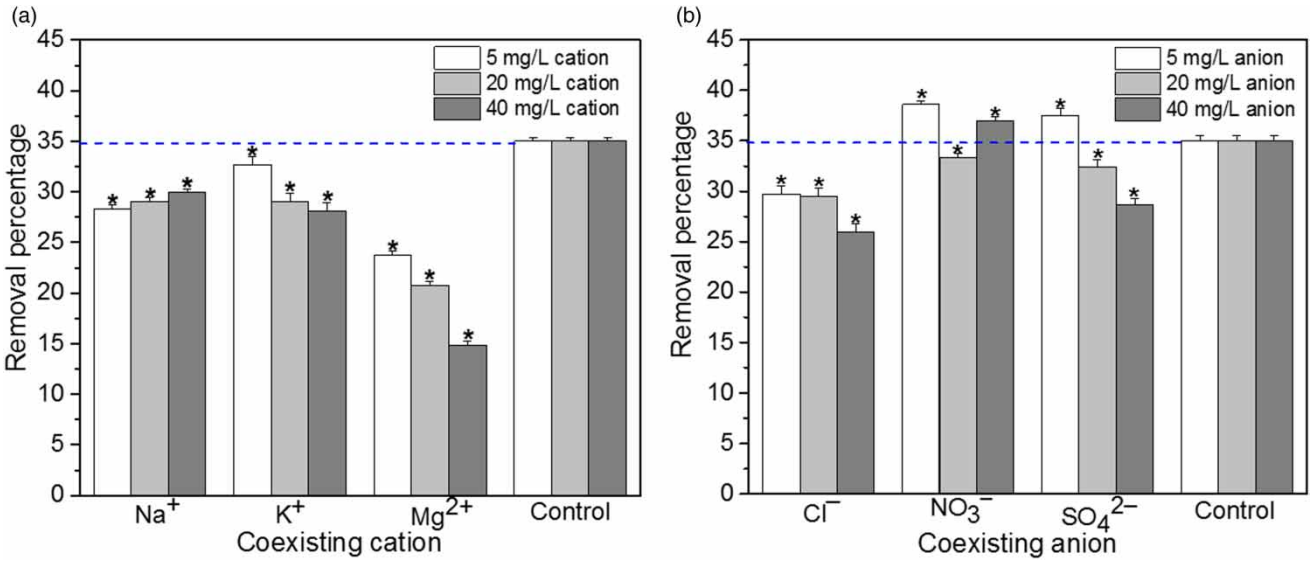

Figure 9 | (a) Effect of the coexisting cation and (b) anion on the adsorption of Cd(II) (initial pH = 7.0, Cd(II) concentration = 20 mg/L, adsorbent dose = 0.5 g, contact time = 8 h, temp. = 298 K, cation and anion concentrations: 5, 20, and 40 mg/L).

et al. 2017). This competition was particularly strong for divalent metal ions (Ca^{2+} or Mg^{2+}), which have same charge as Cd(II) (Li *et al.* 2012), explaining the higher hindering effect of Mg^{2+} compared with K^+ and Na^+.

From Figure 9(b), the presence of Cl^-, NO_3^-, and SO_4^{2-} all made a notable difference ($p < 0.05$) compared with the control at different concentration levels. Cl^- hindered Cd(II) adsorption at the three ion concentration levels used herein, whereas NO_3^- favored Cd(II) adsorption when present at concentrations of 5 and 40 mg/L. SO_4^{2-} increased the Cd(II) removal percentage at lower concentration (5 mg/L). Cl^- is a strong binding ligand in solution via formation of $CdCl_2$ and $CdCl^+$ species (Yao *et al.* 2014). Thus, the adsorption of Cd ions was suppressed in the presence of Cl^-. The enhanced Cd(II) adsorption at low NO_3^- concentration (5 mg/L) can be explained by the anion serving as a ligand and presenting a co-adsorptive effect on the adsorbent (Barot & Bagla 2012). Anions such as NO_3^- and SO_4^{2-} hindered the adsorption of Cd(II) at higher concentration, and this was produced by the higher anionic strength of the metal solution. Thus, the higher anionic strength of the solution affected the activity coefficient of metal ions, limiting the transfer of Cd(II) to the surface of the adsorbent (Chen *et al.* 2009).

Analysis of the surface properties after adsorption

FT-IR can obtain information on certain functional groups present in the structure of the materials and investigate the possible adsorption mechanism. The FT-IR spectra of Fe_3O_4, Fe_3O_4/PP, Fe_3O_4/PP-Cd, and PP are shown in Figure 10. The peak at 570 cm^{-1} belonged to the Fe–O stretching vibration, which was also observed for Fe_3O_4/PP and Fe_3O_4/PP–Cd. PP, a natural polymer, showed a peak at about 2,927 cm^{-1} belonging to O–H stretching. The peak corresponding to C–O stretching appeared at 1,100 and 1,200 cm^{-1}. The spectrum of Fe_3O_4/PP (after PP coating) revealed the presence of C = C vibration (resonance) from the benzene ring. The peak corresponding to this vibration shifted from 1,619 to 1,632 cm^{-1} after PP coating. In addition, the large and intense band of O–H from PP shifted from 3,408 to 3,439 cm^{-1} after PP coating. Therefore, Fe_3O_4 was successfully coated with PP, revealing that the hydroxyl functional groups of PP were covalently bonded to the surface of the magnetite. A new peak could

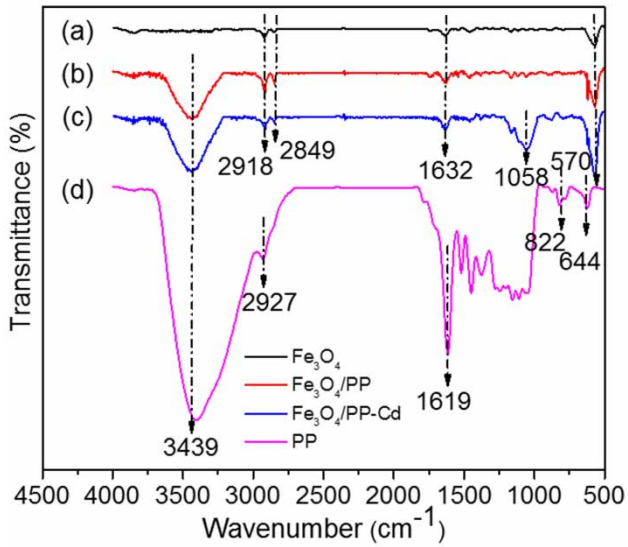

Figure 10 | FT-IR spectra of the (a) Fe_3O_4, (b) Fe_3O_4/PP, (c) Fe_3O_4/PP–Cd, and (d) PP materials.

be seen from the spectrum of Fe_3O_4/PP–Cd (after adsorption of Cd(II)) at 1,058 cm^{-1}, which was tentatively ascribed to the Cd–OH band. It is concluded that the formation of coordination bonds with the hydroxyl functional groups was the main interaction for removal of Cd(II).

XPS was used to identify the surface elements' composition and investigate the adsorption mechanism by analyzing the binding energy changes. The XPS spectra of Fe_3O_4/PP and Fe_3O_4/PP–Cd were obtained to further illustrate the interaction between Cd(II) and Fe_3O_4/PP. The wide scans of Figure 11(a) clearly show Cd 3d peaks at 411.6 and 404.7 eV, also indicating successful adsorption of Cd(II) by Fe_3O_4/PP (Wu *et al.* 2015). The detailed O 1s spectra of Fe_3O_4/PP were deconvoluted into two peaks at 530.0 and 531.5 eV (Figure 11(b)). This is mainly due to metal oxide lattice (Fe–O) and surface hydroxyl (H–O) oxygen species, respectively (Cao *et al.* 2012). After the Cd(II) was adsorbed on Fe_3O_4/PP, the metal oxide lattice oxygen shifted from 530.0 eV to 530.2 eV, while surface hydroxyl groups shifted slightly down by 0.1 eV to 531.4 eV (Figure 11(c)). The decreased binding energy of H–O and the increase of the binding energy of lattice O were indicative of a complexation process between the surface hydroxyl groups and Cd(II) (Zhong *et al.* 2016). As shown in Figure 11(d), the deconvolution of the Cd 3d band resulted in two peaks at 411.3 and 404.6 eV, which

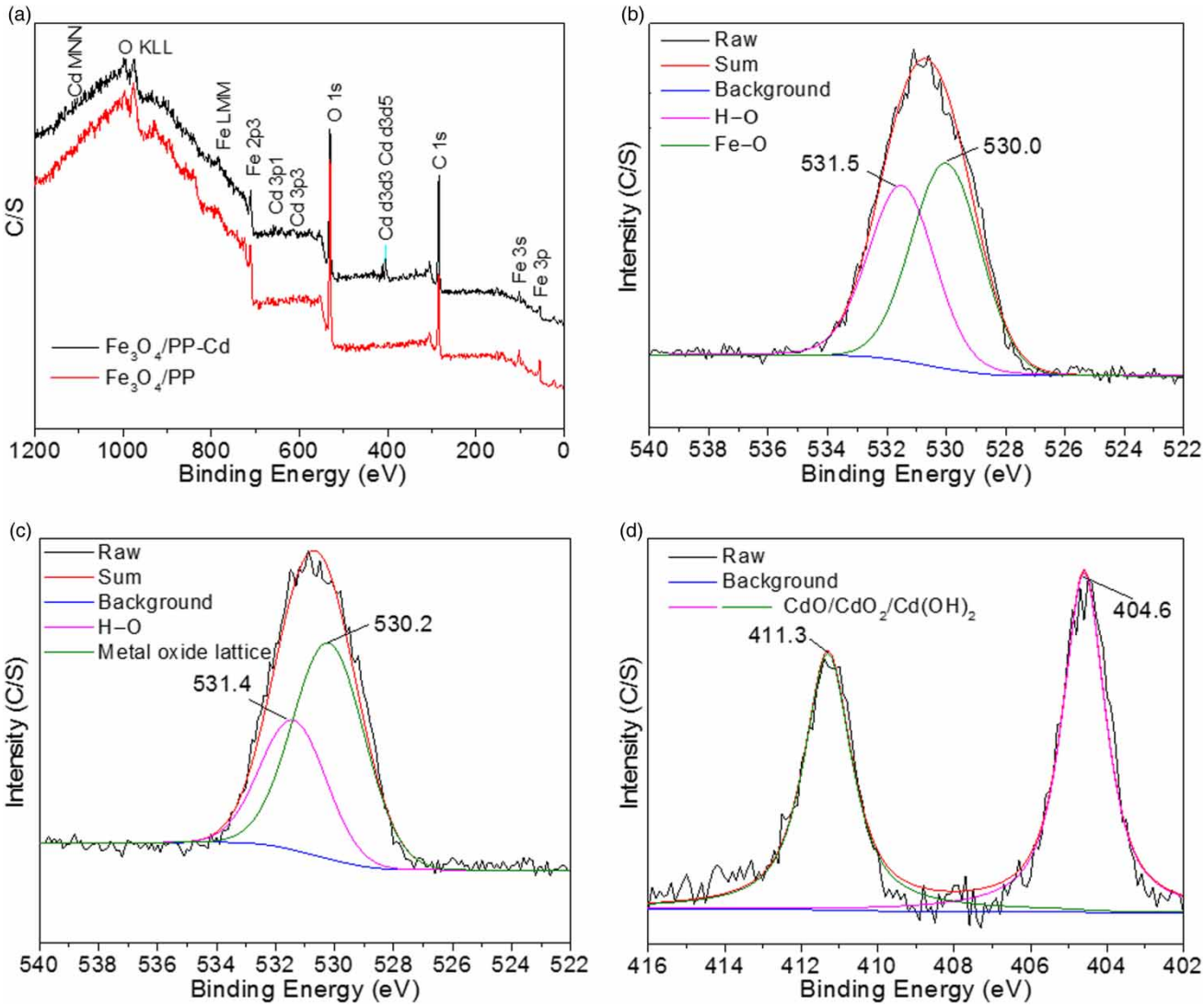

Figure 11 | (a) Wide scans; (b) and (c) O 1s XPS spectra of Fe_3O_4/PP before and after adsorption of Cd(II); (d) Cd 3d XPS spectra of Fe_3O_4/PP after adsorption of Cd(II).

were tentatively ascribed to CdO, CdO_2, $Cd(OH)_2$, or $CdCO_3$ complex species (Ramrakhiani *et al.* 2017). Based on the above analysis, Cd(II) was adsorbed on Fe_3O_4/PP via complexation with hydroxyl groups. In summary, electrostatic interaction (attraction and repulsion) and complexation processes may be involved in the adsorption of Cd(II) on Fe_3O_4/PP.

Practical applications and future perspectives

The raw material of PP powder used in this study is extracted from bark, which is widely distributed in nature. The yield of PP as a kind of natural polymer is large in developing countries. Furthermore, PP is inexpensive as a natural biomass and contains many specific reactive functional groups in its structure. Therefore, it is possible to use PP as a heavy metal adsorbent and it is economically feasible in some developing countries.

The composite adsorbent uses Fe_3O_4 as the core, which gives it superior magnetic properties and can be rapidly separated and recovered from the solution. In general, the separation of common adsorbents from metal solution requires a series of operations (such as filtration, centrifugation, etc.) which increases the treatment cost and the

adsorbents cannot be recycled for further use. With the combination of PP and Fe_3O_4, effective adsorption capacity can be obtained while achieving rapid and easy separation. In addition, compared with other methods, the adsorption method has high efficiency, low cost, and is environmentally friendly.

In this study, the amount of PP coated on the surface of Fe_3O_4 was slightly low and it is necessary to increase the load mass of PP in future research. Fe_3O_4 is obtained from natural magnetite ore and particle size distribution is uneven. Chemical reactions can be considered to control the synthesis process of Fe_3O_4 and reduce particle size, then increase the adsorption efficiency. Actual industrial wastewater is a mixed solution with various heavy metal ions, therefore the removal of multicomponent heavy metals using Fe_3O_4/PP needs to be further explored. In the desorption experiment, the desorption efficiency achieved 75.20% after using 1.0 M HNO_3 and ultrasonication. The degree of corrosion of Fe_3O_4 in 1.0 M HNO_3 was negligible (0.023%), which may result from the property of the natural Fe_3O_4. In order to reuse the Fe_3O_4 it was recoated with PP and the adsorption capacity of Fe_3O_4/PP slightly decreased from 0.70 mg/g to 0.55 mg/g, but stable desorption regeneration was still realized. The slight decrease may be due to the Cd(II) adsorbed on Fe_3O_4. Moreover, the desorbed compound of PP-Cd(II) can be further applied due to the decomposition of PP at high temperature. The concentrated Cd(II) eluent can be used in further industrial processes. The Fe_3O_4/PP achieved good adsorption of Cd(II) in this study and can be recycled easily, which is important from the perspective of cost and practical application. It also indicates the practical application of heavy metal removal from wastewater in developing countries.

CONCLUSIONS

A Fe_3O_4/PP magnetic adsorbent was successfully synthesized by a simple impregnation method. PP was coated on the surface of Fe_3O_4 with an approximate loading of 1.5%. The presence of multiple adjacent phenolic hydroxyls on PP as functional groups allowed effective removal of Cd(II). The adsorption kinetics followed a pseudo second-order model, indicating that the Cd(II) adsorption was controlled by chemical processes. The adsorption isotherm fitted well with the Langmuir model. Thus, the adsorption of Cd(II) was favorable and was carried out by forming a homogeneous monolayer. The adsorption capacity of Cd(II) on Fe_3O_4/PP depended highly on the pH (i.e., the adsorption capacity increased with the pH in the 3.0–8.0 range). The adsorption of Cd(II) was suppressed in the presence of cations and Cl^-, whereas NO_3^- and SO_4^{2-} favored the adsorption of Cd(II) at low concentration (5 mg/L). Thermodynamic studies demonstrated that the Cd(II) adsorption process was spontaneous and endothermic. The adsorption mechanism was mainly controlled by the formation of Cd(II) complexes.

ACKNOWLEDGEMENTS

This work was financially supported by the Chinese National Natural Science Foundation (51672028), Fundamental Research Funds for the Central Universities (2015ZCQ-HJ-02), and Major Science and Technology Program for Water Pollution Control and Treatment (2018ZX07105-001, 2018ZX07110-004).

REFERENCES

Bacelo, H. A. M., Santos, S. C. R. & Botelho, C. M. S. 2016 Tannin-based biosorbents for environmental applications – a review. *Chem. Eng. J.* **303**, 575–587.

Barot, N. S. & Bagla, H. K. 2012 Eco-friendly waste water treatment by cow dung powder (adsorption studies of Cr(III), Cr(VI) and Cd(II) using tracer technique). *Desalin. Water Treat.* **38**, 104–113.

Cao, C. Y., Qu, J., Yan, W. S., Zhu, J. F., Wu, Z. Y. & Song, W. G. 2012 Low-cost synthesis of flowerlike α-Fe_2O_3 nanostructures for heavy metal ion removal: adsorption property and mechanism. *Langmuir* **28**, 4573–4579.

Chand, P., Shil, A. K., Sharma, M. & Pakade, Y. B. 2014 Improved adsorption of cadmium ions from aqueous solution using chemically modified apple pomace: mechanism, kinetics, and thermodynamics. *Int. Biodeter. Biodegr.* **90**, 8–16.

Chang, Z., Yu, Z. G., Zeng, G. M., Huang, B. B., Dong, H. R., Huang, J. H., Yang, Z. Z., Wei, J. J., Hu, L. & Zhang, Q. 2016 Phase transformation of crystalline iron oxides and their adsorption abilities for Pb and Cd. *Chem. Eng. J.* **284**, 247–259.

Chen, C. L., Hu, J., Shao, D. D., Li, J. X. & Wang, X. K. 2009 Adsorption behavior of multiwall carbon nanotube/iron

oxide magnetic composites for Ni(II) and Sr(II). *J. Hazard. Mater.* **164**, 923–928.

Chen, K., He, J. Y., Li, Y. L., Cai, X. G., Zhang, K. S., Liu, T., Hu, Y., Lin, D. Y., Kong, L. T. & Liu, J. H. 2017 Removal of cadmium and lead ions from water by sulfonated magnetic nanoparticle adsorbents. *J. Colloid Interf. Sci.* **494**, 307–316.

Copello, G. J., Pesenti, M. P., Raineri, M., Mebert, A. M., Piehl, L. L., de Celis, E. R. & Diaz, L. E. 2013 Polyphenol-SiO_2 hybrid biosorbent for heavy metal removal. Yerba mate waste (*Ilex paraguariensis*) as polyphenol source: kinetics and isotherm studies. *Colloid Surface. B* **102**, 218–226.

Crini, G. 2005 Recent developments in polysaccharide-based materials used as adsorbents in wastewater treatment. *Prog. Polym. Sci.* **30**, 38–70.

Demiral, H. & Güngör, C. 2016 Adsorption of copper(II) from aqueous solutions on activated carbon prepared from grape bagasse. *J. Clean. Prod.* **124**, 103–113.

Devi, V., Selvaraj, M., Selvam, P., Kumar, A. A., Sankar, S. & Dinakaran, K. 2017 Preparation and characterization of CNSR functionalized Fe_3O_4 magnetic nanoparticles: an efficient adsorbent for the removal of cadmium ion from water. *J. Environ. Chem. Eng.* **5**, 4539–4546.

Dodson, J. R., Parker, H. L., García, A. M., Hicken, A., Asemave, K., Farmer, T. J., He, H., Clark, J. H. & Hunt, A. J. 2015 Bio-derived materials as a green route for precious & critical metal recovery and re-use. *Green Chem.* **46**, 1951–1965.

El-Hamshary, H., Fouda, M. M. G., Moydeen, M. & Al-Deyab, S. S. 2014 Removal of heavy metal using poly (*N*-vinylimidazole)-grafted-carboxymethylated starch. *Int. J. Biol. Macromol.* **66**, 289–294.

Gautam, R. K., Mudhoo, A., Lofrano, G. & Chattopadhyaya, M. C. 2014 Biomass-derived biosorbents for metal ions sequestration: adsorbent modification and activation methods and adsorbent regeneration. *J. Environ. Chem. Eng.* **2**, 239–259.

Gautam, R. K., Sharma, S. K., Mahiya, S. & Chattopadhyaya, M. C. 2015 Contamination of heavy metals in aquatic media: transport, toxicity and technologies for remediation. In: *Heavy Metals In Water: Presence, Removal and Safety* (S. K. Sharma, ed.). The Royal Society of Chemistry, Cambridge, UK, pp. 1–24.

He, L., Gao, S. Y., Wu, H., Liao, X. P., He, Q. & Shi, B. 2012 Antibacterial activity of silver nanoparticles stabilized on tannin-grafted collagen fiber. *Mat. Sci. Eng. C.* **32**, 1050–1056.

Homayoon, F., Faghihian, H. & Torki, F. 2017 Application of a novel magnetic carbon nanotube adsorbent for removal of mercury from aqueous solutions. *Environ. Sci. Pollut.* **2**, 11764–11778.

Huang, X., Liao, X. P. & Shi, B. 2009 Hg(II) removal from aqueous solution by bayberry tannin-immobilized collagen fiber. *J. Hazard. Mater.* **170**, 1141–1148.

Inoue, K., Paudyal, H., Nakagawa, H., Kawakita, H. & Ohto, K. 2010 Selective adsorption of chromium(VI) from zinc(II) and other metal ions using persimmon waste gel. *Hydrometallurgy* **104**, 123–128.

Kim, H. U., Kim, K. H., Chang, Y. Y., Lee, S. M. & Yang, J. K. 2012 Heavy metal removal from aqueous solution by tannins immobilized on collagen. *Desalin. Water Treat.* **48**, 1–8.

Li, X. L., Yang, L. Q., Li, Y. F., Ye, Z. F. & He, A. X. 2012 Efficient removal of Cd^{2+} from aqueous solutions by adsorption on PS-EDTA resins: equilibrium, isotherms, and kinetic studies. *J. Environ. Eng-ASCE* **138**, 940–948.

Machida, M., Fotoohi, B., Amamo, Y. & Mercier, L. 2012 Cadmium(II) and lead(II) adsorption onto hetero-atom functional mesoporous silica and activated carbon. *Appl. Surf. Sci.* **258**, 7389–7394.

Morisada, S., Rin, T., Ogata, T., Kim, Y. H. & Nakano, Y. 2011 Adsorption removal of boron in aqueous solutions by amine-modified tannin gel. *Water Res.* **45**, 4028–4034.

Murithi, G., Onindo, C. O., Wambu, E. W. & Muthakia, G. K. 2014 Removal of cadmium(II) ions from water by adsorption using water hyacinth (*Eichhornia crassipes*) biomass. *Bioresources* **9**, 39–39.

Ping, L., Brosse, N., Chrusciel, L., Navarrete, P. & Pizzi, A. 2011 Extraction of condensed tannins from grape pomace for use as wood adhesives. *Ind. Crop. Prod.* **33**, 253–257.

Ramrakhiani, L., Halder, A., Majumder, A., Mandal, A. K., Majumdar, S. & Ghosh, S. 2017 Industrial waste derived biosorbent for toxic metal remediation: mechanism studies and spent biosorbent management. *Chem. Eng. J.* **308**, 1048–1064.

Roque-Ruiz, J. H., Cabrera-Ontiveros, E. A., Torres-Pérez, J. & Reyes-López, S. Y. 2016 Preparation of PCL/Clay and PVA/Clay electrospun fibers for cadmium (Cd^{+2}), chromium (Cr^{+3}), copper (Cu^{+2}) and lead (Pb^{+2}) removal from water. *Water Air. Soil Poll.* **227**, 1–17.

Shah, J., Jan, M. R., Khan, M. & Amir, S. 2016 Removal and recovery of cadmium from aqueous solutions using magnetic nanoparticle-modified sawdust: kinetics and adsorption isotherm studies. *Desalin. Water Treat.* **57**, 9736–9744.

Silva, F. A. & Pissetti, F. L. 2014 Adsorption of cadmium ions on thiol or sulfonic-functionalized poly(dimethylsiloxane) networks. *J. Colloid Interf. Sci.* **416**, 95–100.

Singh, D., Gautam, R. K., Kumar, R., Shukla, B. K., Shankar, V. & Krishna, V. 2014 Citric acid coated magnetic nanoparticles: synthesis, characterization and application in removal of Cd(II) ions from aqueous solution. *J. Water Process Eng.* **4**, 233–241.

Venkateswarlu, S. & Yoon, M. 2015 Rapid removal of cadmium ions using green-synthesized Fe_3O_4 nanoparticles capped with diethyl-4-(4 amino-5-mercapto-4*H*-1,2,4-triazol-3-yl) phenyl phosphonate. *RSC Adv.* **5**, 65444–65453.

Wang, L., Liang, W. Y., Yu, J., Liang, Z. X., Ruan, L. L. & Zhang, Y. C. 2013 Flocculation of *Microcystis aeruginosa* using modified larch tannin. *Environ. Sci. Technol.* **47**, 5771–5777.

Wang, X. Y., Zhao, Y., Jiang, X. X., Liu, L. J., Li, H. X. & Liang, W. Y. 2018 *In-situ* self-assembly of plant polyphenol-coated Fe_3O_4 particles for oleaginous microalgae harvesting. *J. Environ. Manage.* **214**, 335–345.

Wu, S. B., Zhang, K. S., Wang, X. L., Jia, Y., Sun, B., Luo, T., Meng, F. L., Jin, Z., Lin, D. Y., Shen, W., Kong, L. T. & Liu, J. H. 2015

Enhanced adsorption of cadmium ions by 3D sulfonated reduced graphene oxide. *Chem. Eng. J.* **262**, 1292–1302.

Xie, F., Fan, R., Yi, Q., Zhang, Q. & Lou, Z. 2016 NaOH modification of persimmon powder-formaldehyde resin to enhance Cu^{2+} and Pb^{2+} removal from aqueous solution. *Procedia. Environ. Sci.* **262**, 1292–1302.

Xu, P., Zeng, G. M., Huang, D. L., Lai, C., Zhao, M. H., Wei, Z., Li, N. J., Huang, C. & Xie, G. X. 2012 Adsorption of Pb(II) by iron oxide nanoparticles immobilized *Phanerochaete chrysosporium*: equilibrium, kinetic, thermodynamic and mechanisms analysis. *Chem. Eng. J.* **203**, 423–431.

Xu, L. L., Chen, J., Wen, Y. Z., Li, H., Ma, J. Q. & Fu, D. M. 2016 Fast and effective removal of cadmium ion from water using chitosan encapsulated magnetic Fe_3O_4 nanoparticles. *Desalin. Water Treat.* **57**, 8540–8548.

Xu, Q. H., Wang, Y. L., Jin, L. Q., Wang, Y. & Qin, M. H. 2017 Adsorption of Cu (II), Pb (II) and Cr (VI) from aqueous solutions using black wattle tannin-immobilized nanocellulose. *J. Hazard. Mater.* **339**, 91–99.

Yao, S. H., Liu, Z. R. & Shi, Z. L. 2014 Adsorption behavior of cadmium ion onto synthetic ferrihydrite: effects of pH and natural seawater ligands. *J. Iran. Chem. Soc.* **11**, 1545–1551.

Yurtsever, M. & Sengil, I. A. 2009 Biosorption of Pb(II) ions by modified quebracho tannin resin. *J. Hazard. Mater.* **163**, 58–64.

Zeng, G. M., Liu, Y. Y., Tang, L., Yang, G. D., Pang, Y., Zhang, Y., Zhou, Y. Y., Li, Z., Li, M., Lai, M., He, X. & He, Y. 2015 Enhancement of Cd(II) adsorption by polyacrylic acid modified magnetic mesoporous carbon. *Chem. Eng. J.* **259**, 153–160.

Zhai, Y. & Wang, H. 2015 Kinetics and mechanism study on adsorption of cadmium by freshly synthesized hydrous manganese dioxide. *Desalin. Water Treat.* **26**, 1–10.

Zhong, L. B., Yin, J., Liu, S. G., Liu, Q., Yang, Y. S. & Zheng, Y. M. 2016 Facile one-pot synthesis of urchin-like Fe–Mn binary oxide nanoparticles for effective adsorption of Cd(II) from water. *RSC Adv.* **6**, 103438–103445.

First received 16 April 2018; accepted in revised form 10 August 2018. Available online 21 September 2018